

THE NEUTRAL HYDROGEN DISTRIBUTION IN MERGING GALAXIES: DIFFERENCES BETWEEN STELLAR AND GASEOUS TIDAL MORPHOLOGIES

J. E. HIBBARD¹

National Radio Astronomy Observatory², 520 Edgemont Road, Charlottesville, VA, 22903;

jhibbard@nrao.edu

W. D. VACCA

IRTF, Institute for Astronomy, 2680 Woodlawn Drive, Honolulu, HI 96822; vacca@ifa.hawaii.edu

M. S. YUN

National Radio Astronomy Observatory², P.O. Box 0, Socorro, New Mexico, 87801; myun@nrao.edu

To appear in the March 2000 issue of The Astronomical Journal

ABSTRACT

As part of several H I synthesis mapping studies of merging galaxies, we have mapped the tidal gas in the three disk-disk merger systems Arp 157 (NGC 520), Arp 220, and Arp 299 (NGC 3690). These systems differ from the majority of the mergers mapped in H I, in that their stellar and gaseous tidal features do not coincide. In particular, they exhibit large stellar tidal features with little if any accompanying neutral gas and large gas-rich tidal features with little if any accompanying starlight. On smaller scales, there are striking anti-correlations where the gaseous and stellar tidal features appear to cross. We explore several possible causes for these differences, including dust obscuration, ram pressure stripping, and ionization effects. No single explanation can account for all of the observed differences. The fact that each of these systems shows evidence for a starburst driven superwind expanding in the direction of the most striking anti-correlations leads us to suggest that the superwind is primarily responsible for the observed differences, either by sweeping the features clear of gas via ram pressure, or by excavating a clear sightline towards the starburst and allowing UV photons to ionize regions of the tails. If this suggestion is correct, only systems hosting a galactic superwind and experiencing a high-inclination encounter geometry (such that tidal gas is lifted high above the starburst regions) should exhibit such extreme differences between their H I and optical tidal morphologies.

Subject headings: galaxies: individual (Arp 220, NGC 3690, NGC 520) — galaxies: interactions — galaxies: ISM — galaxies: peculiar — galaxies: starburst —

1. INTRODUCTION

Nearly 30 years ago, Toomre & Toomre (1972) elegantly demonstrated that the tails and bridges emanating from many peculiar galaxies may arise kinematically from dynamically cold disk material torn off of the outer regions of galaxies experiencing strong gravitational interactions. Early spectroscopic studies of gas within the tidal tails of merging galaxies provided observational support for this hypothesis by showing the tails to have the kinematics expected for a gravitational origin (e.g. Stockton 1974a,b). H I mapping studies are particularly well suited to such studies, as the tidally ejected disk material is usually rich in neutral hydrogen and can be traced to very large distances from the merging systems (e.g. van der Hulst 1979; Simkin *et al.* 1986; Appleton *et al.* 1981, 1987; Yun *et al.* 1994). Once mapped, the tidal kinematics can be used either alone, to disentangle the approximate spin geometry of the encounter (Stockton 1974a,b; Mihos *et al.* 1993; Hibbard & van Gorkom 1996, hereafter HvG96; Mihos & Bothun 1998), or in concert with detailed numerical models, to constrain the full encounter geometry (e.g. Combes 1978; Combes *et al.* 1988; Yun 1992, 1997; Hibbard &

Mihos 1995; Gardiner & Noguchi 1996).

However, not all systems can be easily explained by purely gravitational models such as those used by Toomre & Toomre. For example, gravitational forces by themselves should not lead to differences between stellar and gaseous tidal components. Numerical models which include hydrodynamical effects do predict a decoupling of the dissipative gaseous and non-dissipative stellar components (e.g. Noguchi 1988; Barnes & Hernquist 1991, 1996; Weil & Hernquist 1993; Mihos & Hernquist 1996; Appleton, Charmandaris & Struck 1996; Struck 1997), but only in the inner regions or along bridges where gas orbits may physically intersect (see e.g. Fig. 4 of Mihos & Hernquist 1996). Decoupling of the gaseous and stellar components within the tidal tails is not expected.

Nonetheless, differences between the optical and gaseous tidal morphologies have been observed. These differences can be subtle, with the peak optical and H I surface brightnesses simply displaced by a few kpc within the tails (e.g. NGC 4747, Wevers *et al.* 1984; NGC 2782 Smith 1994; NGC 7714/4 Smith *et al.* 1997; Arp 295A, NGC 4676B, and NGC 520 Southern tail, Hibbard 1995, HvG96), or they can be extreme, with extensive H I tidal features ap-

¹Visiting Astronomer, Kitt Peak National Observatory, National Optical Astronomy Observatories, which is operated by the Association of Universities for Research in Astronomy, Inc. (AURA) under cooperative agreement with the National Science Foundation.

²The National Radio Astronomy Observatory is operated by Associated Universities, Inc., under cooperative agreement with the National Science Foundation.

parently decoupled from, or even anti-correlated with, the optical tidal features. It is this latter category of objects that we wish to address in this paper. In particular, we address the morphology of the tidal gas and starlight in the merging systems NGC 520 (Arp 157), Arp 220, and Arp 299 (NGC 3690).

The three systems were observed as part of our on-going studies on the tidal morphologies of optically and IR selected mergers (Hibbard 1995, HvG96, Hibbard & Yun 1996 and in prep.). These studies involve moderate resolution ($\theta_{FWHM} \sim 15''$) VLA HI spectral-line mapping observations and deep optical *B* and *R* broad-band imaging with large format CCDs using the KPNO 0.9m (NGC 520) and the University of Hawaii 88'' telescopes. The HI and optical observations, reduction, and data products have been presented in Hibbard (1995) and HvG96 for NGC 520, in Hibbard & Yun (1999, hereafter HY99) for Arp 299, and in Yun & Hibbard (2000; see also Hibbard & Yun 1996) for Arp 220. We refer the reader to these papers for details of the observations and data reduction. These systems are extremely disturbed, and we cannot hope to offer a full description of their peculiarities here. For more information we refer the reader to the above references.

2. OBSERVED STELLAR AND GASEOUS TIDAL MORPHOLOGIES

Figures 1–3 show the optical and atomic gas morphologies of each of the three systems discussed here. For NGC 520 and Arp 220 only the inner regions are shown in order to highlight the differences we wish to address. Panel (a) presents a greyscale representation of the optical morphology of each system with features of interest labeled. Panel (b) shows the HI distribution. Contours indicate the distribution of HI mapped at low-resolution ($\theta_{FWHM} \sim 30''$), whereas the greyscales show the HI mapped at higher resolution ($\theta_{FWHM} \sim 15''$). The former is sensitive to diffuse low column density (N_{HI}) neutral hydrogen, while the latter delineates the distribution of the higher column density HI. The central region of each HI map appears to have a hole (indicated by the dotted contours), which is due to HI absorption against the radio continuum associated with the disk-wide starbursts taking place in each galaxy (see Condon *et al.* 1990). In panel (c), we again present the optical morphology in greyscales, and the higher resolution HI distribution as contours. Finally, panel (d) presents a smoothed, star-subtracted *R*-band image contoured upon a greyscale representation of the high-resolution HI map.

In the final panels of Figs. 1–3 dashed lines labeled “Slice” indicate the locations from which HI and optical intensity profiles have been extracted; these profiles are plotted in Figure 4. Arrows labeled “Superwind” indicate the position angle (P.A.) of H α or soft x-ray plumes, believed to arise from a starburst-driven outflow or galactic superwind in each system. Such outflows are common in other IR bright starbursts (e.g. Heckman, Armus & Miley

1987, 1990 hereafter HAM90; Armus, Heckman, & Miley 1990; Lehnert & Heckman 1996), and are thought to arise when the mechanical energy from massive stars and supernovae in the central starburst is sufficient to drive the dense interstellar medium outward along the minor axis (e.g. Chevalier & Clegg 1985; Joseph & Wright 1985; Suchkov *et al.* 1994). Often, such starbursts are powerful enough to drive a freely expanding wind of hot plasma completely out of the galaxy (“blowout”; HAM90).

In the following subsections we briefly discuss what is known about the dynamical state of each system, and describe the differences between the stellar and gaseous tidal morphologies. Throughout this paper distances and other physical properties are calculated assuming $H_0 = 75 \text{ km s}^{-1} \text{ Mpc}^{-1}$.

2.1. NGC 520

NGC 520 (Arp 157, UGC 966) is an intermediate-stage merger, with the two progenitor nuclei separated by $40''$ (5.8 kpc for $D = 30 \text{ Mpc}$, $1'' = 145 \text{ pc}$) and embedded within a common luminous envelope (HvG96 and references therein; see Fig. 1a). There is a bright optical tidal tail stretching 24 kpc to the southeast (henceforth referred to as the S Tail) which bends sharply eastward and connects onto a broad optical plume³. This plume continues to the north and west for 60 kpc before it appears to connect onto extended light surrounding the dwarf galaxy UGC 957 (outside the region plotted in Fig. 1a; see Stockton & Bertola 1980).

The primary nucleus (the easternmost nucleus in Fig. 1a) possesses a massive ($\sim 5 \times 10^9 M_\odot$) 1 kpc-scale rotating molecular gas disk (Sanders *et al.* 1988; Yun & Hibbard 1999). An HI disk is kinematically centered on this molecular disk, and extends to a radius of $\sim 20 \text{ kpc}$ (labeled “Inner Disk” in Fig. 1b). Beyond this there is an intermediate ring of HI with a mean radius of $\sim 30 \text{ kpc}$ (i.e., the material which contains the feature labeled “N Clump” in Fig. 1b), and a nearly complete outer ring of HI with a mean radius of 60 kpc, which extends smoothly through the dwarf galaxy⁴ UGC 957 (only partially seen in Fig. 1b). There is a kinematic and morphological continuity between the molecular gas disk, the inner HI disk, and outer HI ring (Yun & Hibbard 1999), which suggests that all of this material is associated with the primary nucleus.

The observations suggests that the NGC 520 interaction involved a prograde-retrograde or prograde-polar spin geometry: The linear morphology of the optical tail-to-plume system is typical of features produced by a disk experiencing a prograde encounter (i.e., the disk rotates in the same direction as the merging systems orbit each other). The disk-like morphology and rotational kinematics of the large-scale HI and the lack of any aligned linear tidal features, on the other hand, are more typical of polar or retrograde encounter geometries (i.e., disk rotation either perpendicular to or opposite the direction of orbital motion). Such encounters fail to raise significant tails (Toomre & Toomre 1972; Barnes 1988), and much of

³We follow the naming convention of Schombert *et al.* 1990 and refer to tidal features with flat intensity profiles as plumes, and ones with Gaussian profiles as tails

⁴The HI kinematics show that UGC 957 is kinematically associated with this outer gas ring, although it may lie slightly above or below it. Rudimentary numerical modeling has shown that it is unlikely that the UGC galaxy is responsible for the main optical features of the NGC 520 system (Stanford & Balcells 1991). It is unclear whether this system is an interloper or was recently assembled from the surrounding ring of gas.

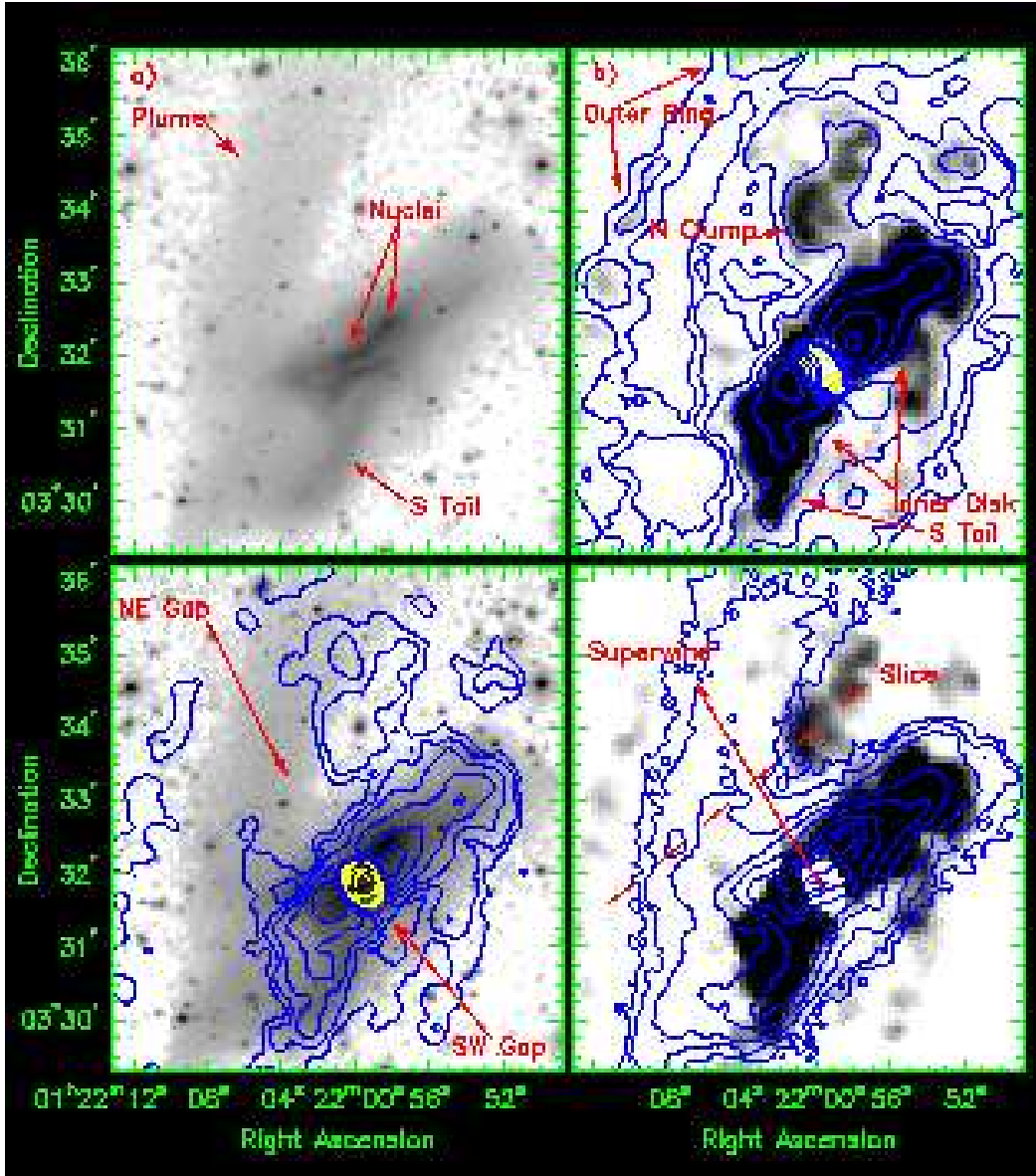


FIG. 1.— HI AND OPTICAL MORPHOLOGY OF NGC 520. Panel (a) (top left) displays an R -band image with features of interest labeled. Panel (b) (upper right) presents a greyscale and contour representation of the HI data. The contours indicate the distribution of HI mapped at low-resolution ($\theta_{FWHM} \sim 25''$), whereas the greyscales show the HI mapped at higher resolution ($\theta_{FWHM} \sim 17''$). The lowest contour is drawn at a column density of $5 \times 10^{19} \text{ cm}^{-2}$, with successive contours a factor of 2 higher. The greyscales range from $1 \times 10^{20} \text{ cm}^{-2}$ (white) to $4 \times 10^{20} \text{ cm}^{-2}$ (black). Panel (c) (lower left) presents the optical image in greyscales with contours from the high-resolution HI data superimposed. The lowest contour is drawn at a column density of $1 \times 10^{20} \text{ cm}^{-2}$, with successive contours a factor of 2 higher. Panel (d) (lower right) shows contours from a star-subtracted R -band image (lowest contour of $27 \text{ mag arcsec}^{-2}$ and contour interval of $1 \text{ mag arcsec}^{-2}$) upon greyscales of the high-resolution HI data (from $1 \times 10^{20} \text{ cm}^{-2}$ to $4 \times 10^{20} \text{ cm}^{-2}$). The dashed line labeled “Slice” indicates the locations of the intensity profiles plotted in Fig. 4a. The arrow labeled “Superwind” indicates the direction (but not the extent) of the putative expanding superwind.

the disk material remains close to its original rotational plane.

Neither the intermediate nor the outer HI ring has an optical counterpart ($\mu_R > 27 \text{ mag arcsec}^{-2}$). Despite smooth rotational kinematics, this outer HI has a very clumpy and irregular morphology, with notable gaps near

the optical minor axis (labeled “NE gap” and “SW gap” in Fig. 1c). This figure shows that the outer HI and optical structures are anti-correlated, with the peak HI column densities (associated with the N clump) located to one side of the optical plume. In Fig. 1d the HI clump appears to be bounded on three sides by the optical con-

tours. In Fig. 4a we present an intensity profile at the location indicated by the dotted line in Fig. 1d, showing that the gas column density increases precisely where the optical light decreases.

While the HI features exhibit a clear rotational kinematic signature, the well-defined edges and nearly-linear structure of the optical plume suggests that its constituent stars are moving predominantly along the plume, rather than in the plane of the sky: any substantial differential rotation would increase the width of the plume and result in a more disk-like morphology. We therefore conclude that the gas rings and optical plume are both morphologically and kinematically distinct entities. This suggests that the observed gas/star anti-correlation is either transient (and fortuitous) or actively maintained by some process.

A deep H α image of NGC 520 shows plumes of ionized gas emerging both north and south along the minor axis and reaching a projected height of 3 kpc from the nucleus (HvG96). It has been suggested that this plume represents a starburst-driven outflow of ionized gas (HvG96, Norman *et al.* 1996). The position angle of this plume is indicated by an arrow in Fig. 4d (P.A. = 25°). This direction corresponds to the most dramatic HI/optical anti-correlations mentioned above, and in the following we suggest that this region of the optical tail actually lies directly in the path of the out-flowing wind.

2.2. Arp 299

Arp 299 (NGC 3690/IC 694, UGC 6471/2, Mrk 171, VV 118) is also an intermediate stage merger, with two disk systems (IC 694 to the east, NGC 3690 to the west — see Figure 2a) in close contact but with their respective nuclei separated by 20'' (4.7 kpc for $D=48$ Mpc, 1'' = 233 pc). A long, narrow, faint ($\mu_R \gtrsim 26$ mag arcsec $^{-2}$) tidal tail stretches to the north to a radius of ~ 125 kpc. HI imaging of this system by HY99 (see also Nordgren *et al.* 1997) shows a rotating gas-rich disk within the inner regions, and a pair of parallel HI filaments extending to the north. From the HI morphology and kinematics, HY99 deduce that Arp 299 is the result of a prograde-retrograde or prograde-polar encounter between two late-type spirals, with the inner HI disk associated with the retrograde disk of IC 694, and the northern optical tail and tidal HI filaments ejected by the prograde disk of NGC 3690.

The parallel-filament or bifurcated morphology of the tidal HI is quite unlike that of the optical tail. The inner HI filament (so labeled in Fig. 2b) is of lower characteristic column density ($N_{HI} \lesssim 8 \times 10^{19}$ cm $^{-2}$) and is associated with the low surface brightness stellar tail (Fig. 2c). The gas in this filament has a more irregular morphology than that in the outer filament (e.g., the “gap” and “knot” in Fig. 2b), and much of this material is detectable only after a substantial smoothing of the data (Fig. 2b). The outer filament is characterized by a higher HI column density ($N_{HI} \sim 1.5 \times 10^{20}$ cm $^{-2}$) but has no optical counterpart ($\mu_R > 27.5$ mag arcsec $^{-2}$). This filament is displaced by approximately 20 kpc (in projection) to the west of the inner filament for much its length, after which the filaments merge together in a feature labeled the “N Clump” in Fig. 2b. The parallel filaments have nearly identical

kinematics along their entire lengths, and join smoothly at the N Clump. This implies that these features form a single physical structure.

Based on preliminary numerical simulations, HY99 suggest that a bifurcated morphology can arise quite naturally during tail formation. This occurs when the optically faint, gas-rich outer regions of the progenitor disk are projected adjacent to optically brighter regions coming from smaller initial radii⁵ (see also Mihos, 2000). However, this scenario does not explain why the inner filament, presumably drawn from optically bright but still gas-rich material within the optical disk of the progenitor, should lack accompanying HI.

As in NGC 520, there is an anti-correlation between the optical and gaseous column densities across the N clump, with the highest gas column densities ($2\text{--}3 \times 10^{20}$ cm $^{-2}$) located on either side of the optical tail. This is illustrated in Fig. 4b, where we plot a profile along the position indicated by the dotted line in Fig. 2d. The optical tail emerges above the N clump, and appears to curve exactly around the northern edge of the N clump (labeled “hook” in Fig. 2c). Also labeled in Fig. 2c are the three regions with anomalously high HI velocity dispersions noted by HY99 ($\sigma_{HI} \sim 13\text{--}20$ km s $^{-1}$ compared with $\sigma_{HI} \sim 7\text{--}10$ km s $^{-1}$ for the remainder of the tail; see Fig. 7d of HY99); we will refer to these regions in the discussion (§ 3.4.2).

Within the main body of Arp 299, vigorous star formation is taking place, with an inferred star formation rate (SFR) of $50 M_{\odot} \text{ yr}^{-1}$ (HAM90). Recent X-ray observations reported by Heckman *et al.* (1999) show evidence for hot gas emerging from the inner regions and reaching 25 kpc to the north, which the authors interpret as evidence for a hot, expanding superwind. The position angle of this feature (P.A.=25°) is indicated by the arrow in Fig. 2d, and points towards the inner tidal filament and N clump.

2.3. Arp 220

Arp 220 (UGC 9913, IC 4453/4) is the prototypical ultraluminous infrared galaxy with $L_{8\text{--}100\mu\text{m}} = 1.5 \times 10^{12} L_{\odot}$ (Soifer *et al.* 1984). It is an advanced merger system with two radio and infrared nuclei separated by 0.9'' (345 pc for $D=79$ Mpc), and a bright optical plume extending 35 kpc to the NW (Fig. 3a). Each of the two nuclei has its own compact molecular disk. The two nuclear disks are in turn embedded in one larger 1 kpc scale molecular gas disk (see Scoville, Yun, & Bryant 1997, Downes & Solomon 1998, Sakamoto *et al.* 1999 and references therein). The spin axis of the eastern nucleus is aligned with that of the kpc-scale disk while the western nucleus rotates in the opposite direction. These observations suggest that Arp 220 is the product of a prograde-retrograde merger of two gas rich spiral galaxies (Scoville, Yun, & Bryant 1997).

An irregular disk-like distribution of neutral hydrogen extends over a 100 kpc diameter region surrounding the optical galaxy (Yun & Hibbard 1999a). The overall HI kinematics indicates that this material has a component of rotation in the same sense as that for the eastern nucleus and the molecular gas disk, and opposite the rotation of the western nucleus. This suggests that the HI disk and eastern nucleus originated from the retrograde progenitor, while the western nucleus and NW optical plume

⁵To produce filaments as well separated as found in Arp 299 HY99 suggest that the bifurcation is exacerbated by a pre-existing gaseous warp in the progenitor disk.

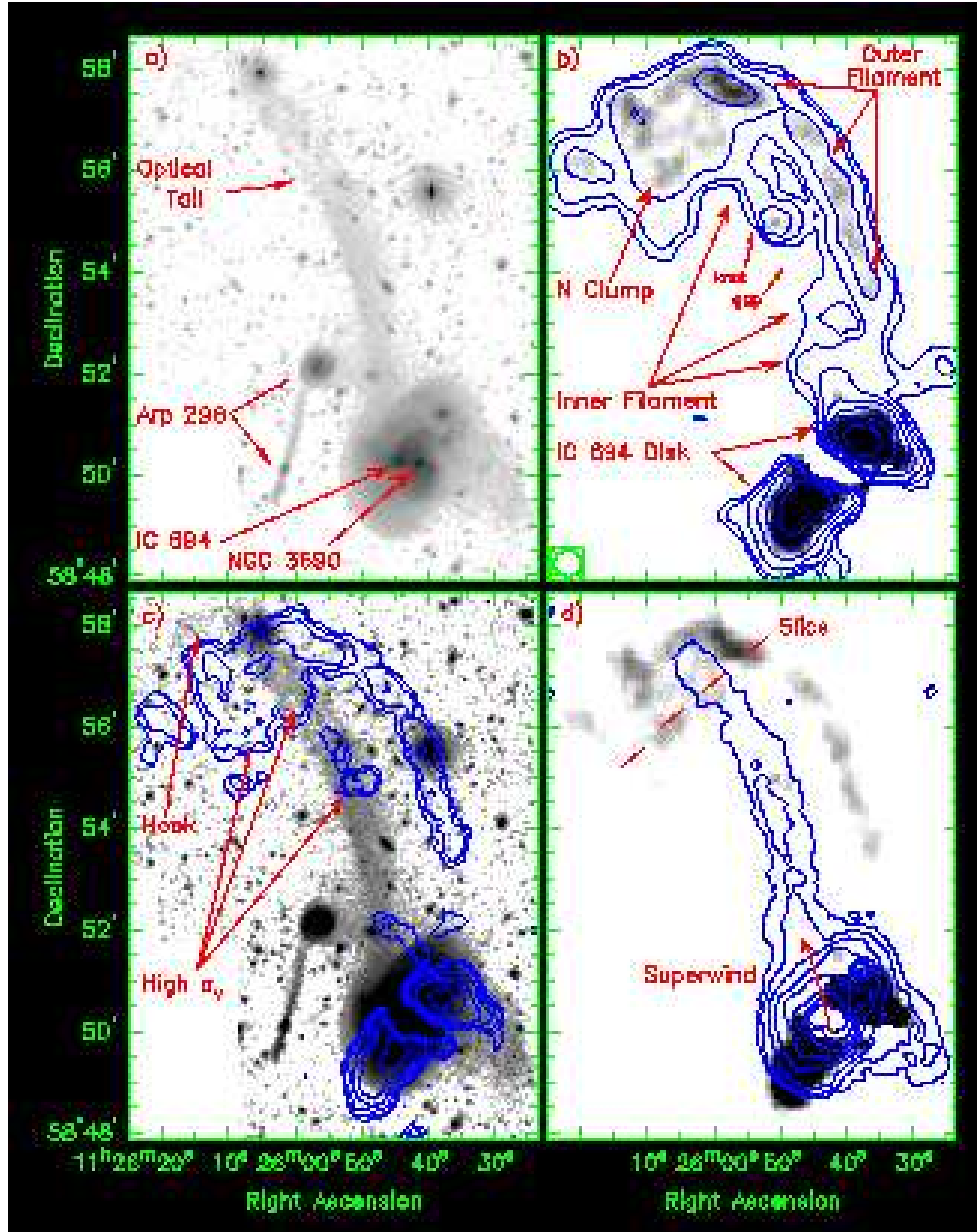


FIG. 2.— HI AND OPTICAL MORPHOLOGY OF ARP 299. Panel (a) (top left) displays an R -band image with features of interest labeled. Panel (b) (upper right) presents a greyscale and contour representation of the HI data. The contours indicate the distribution of HI mapped at low-resolution ($\theta_{FWHM} \sim 35''$), whereas the greyscales show the HI mapped at higher resolution ($\theta_{FWHM} \sim 20''$). The lowest contour is drawn at a column density of $2.5 \times 10^{19} \text{ cm}^{-2}$, with successive contours a factor of 2 higher. The greyscales range from $1 \times 10^{20} \text{ cm}^{-2}$ (white) to $4 \times 10^{20} \text{ cm}^{-2}$ (black). Panel (c) (lower left) presents the optical image in greyscales with contours from the high-resolution HI data superimposed. The lowest contour is drawn at a column density of $5 \times 10^{19} \text{ cm}^{-2}$, with successive contours a factor of 2 higher. Panel (d) (lower right) shows contours from a star-subtracted R -band image (lowest contour of $27 \text{ mag arcsec}^{-2}$ and contour interval of $1 \text{ mag arcsec}^{-2}$) upon greyscales of the high-resolution HI data (from $1 \times 10^{20} \text{ cm}^{-2}$ to $4 \times 10^{20} \text{ cm}^{-2}$). The dashed line labeled “Slice” indicates the locations of the intensity profiles plotted in Fig. 4b. The arrow labeled “Superwind” indicates the direction (but not the extent) of the putative expanding superwind.

(Fig. 3a) arose from the prograde progenitor.

Because of the vigorous star formation occurring within Arp 220 ($\text{SFR} = 340 M_{\odot} \text{ yr}^{-1}$, HAM90), much of the HI within the optical body of the system is seen only in ab-

sorption against the bright radio continuum emission from the central starburst. Beyond this, the HI has high column densities ($N_{HI} \sim 1.5 \times 10^{20} \text{ cm}^{-2}$), but only to the NE and SW. Most notably, there are local HI minima to the

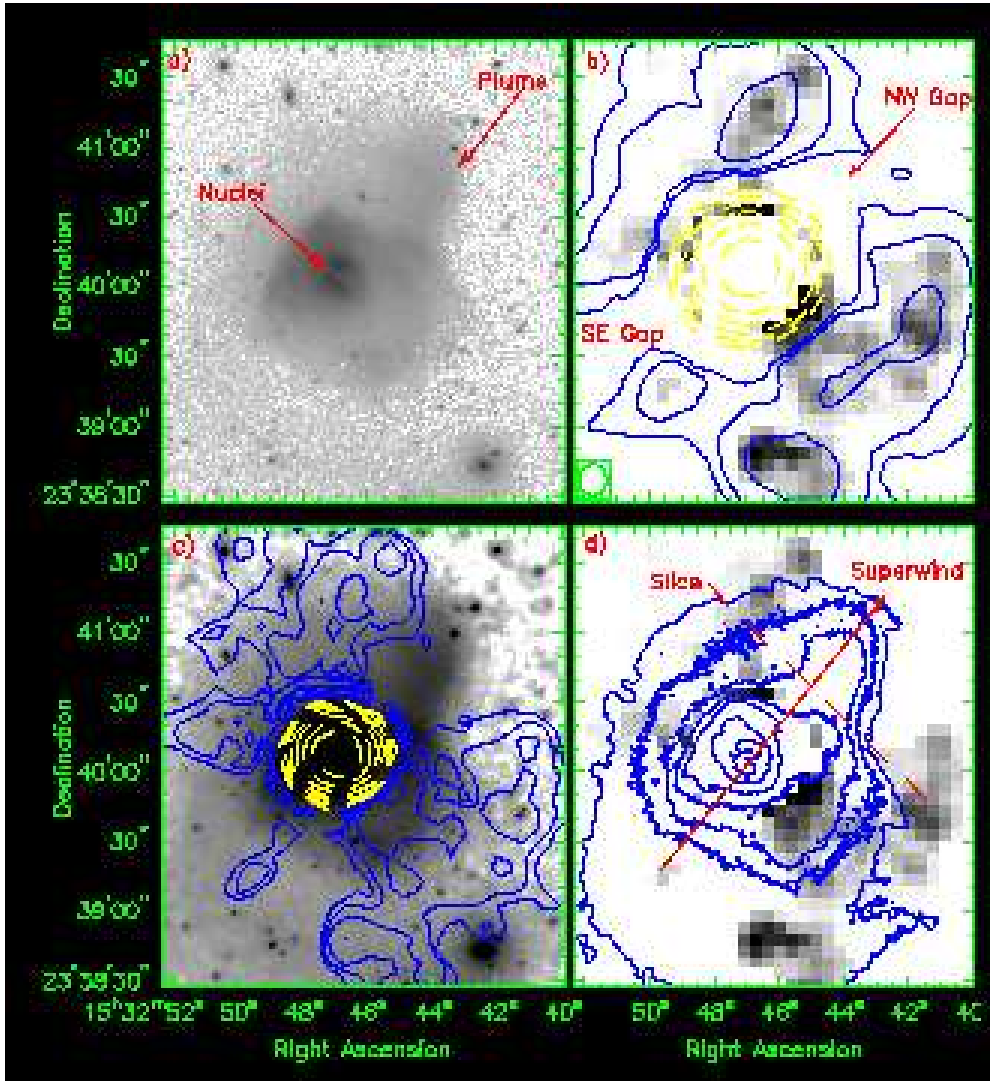


FIG. 3.— HI AND OPTICAL MORPHOLOGY OF ARP 220. Panel (a) (top left) displays an R -band image with features of interest labeled. Panel (b) (upper right) presents a greyscale and contour representation of the HI data. The contours indicate the distribution of HI mapped at low-resolution ($\theta_{FWHM} \sim 30''$), whereas the greyscales show the HI mapped at higher resolution ($\theta_{FWHM} \sim 18''$). The lowest contour is drawn at a column density of $5 \times 10^{19} \text{ cm}^{-2}$, with successive contours a factor of 2 higher. The greyscales range from $1 \times 10^{20} \text{ cm}^{-2}$ (white) to $4 \times 10^{20} \text{ cm}^{-2}$ (black). Panel (c) (lower left) presents the optical image in greyscales with contours from the high-resolution HI data superimposed. The lowest contour is drawn at a column density of $5 \times 10^{19} \text{ cm}^{-2}$, with successive contours a factor of 2 higher. Panel (d) (lower right) shows contours from a star-subtracted R -band image (lowest contour of $26 \text{ mag arcsec}^{-2}$ and contour interval of $1 \text{ mag arcsec}^{-2}$) upon greyscales of the high-resolution HI data (from $1 \times 10^{20} \text{ cm}^{-2}$ to $4 \times 10^{20} \text{ cm}^{-2}$). The dashed line labeled “Slice” indicates the locations of the intensity profiles plotted in Fig. 4c. The arrow labeled “Superwind” indicates the direction (but not the extent) of the putative expanding superwind.

NW and SE (see gaps in Fig. 3b). Comparison of the HI map with the optical image (Fig. 3c) shows that the NW gap occurs exactly at the location of the optical tail. The relationship between the optical and HI surface brightness levels across this feature are illustrated by an intensity profile measured along the dotted line shown in Fig. 3d, and plotted in Fig. 4c. As in NGC 520 and Arp 299, the gas column density increases precisely where the optical light

from the tail begins to fall off. There is a similar HI gap to the SE, but in this case there is no corresponding optical feature associated with it. At even larger radii, the HI is more diffuse ($N_{HI} \sim 3 \times 10^{19} \text{ cm}^{-2}$) and has no optical counterpart down to $\mu_R = 27 \text{ mag arcsec}^{-2}$.

An X-ray image obtained with the ROSAT HRI camera (Heckman *et al.* 1996) reveals an extended central source that is elongated along P.A. = 135° (indicated by arrows in

Fig. 3). A deep $H\alpha + [N II]$ image of Arp 220 reveals ionized gas with a bright linear morphology at this same position angle (Heckman, Armus & Miley 1987). The optical emission line kinematics are suggestive of a bipolar outflow (HAM90), and the physical properties of the warm and hot gas strongly support the superwind scenario for this emission (HAM90, Heckman *et al.* 1996). As in NGC 520 and Arp 299, the position angle of the putative expanding superwind is in the same direction as the H I minima, i.e. NW and SE.

3. DISCUSSION

Figures 1–4 provide evidence for both small- and large-scale differences in the distributions of the tidal gas and stars in these three systems. The small-scale differences are of the type illustrated in Fig. 4, whereby the gas column density falls off just as the optical surface brightness increases at various edges of the tidal features. In NGC 520 and Arp 220, the large-scale differences are between the outer H I rings and disks (which have no associated starlight) and the optical tails and plumes (which have no associated H I). Although these features are kinematically decoupled at present (with the gas rings and disks predominantly in rotation and the optical tails and plumes predominantly in expansion), it is possible that they had a common origin and have subsequently decoupled and evolved separately. In Arp 299, on the other hand, the H I filaments and optical tail have similar morphologies and continuous kinematics and are therefore part of the same kinematic structure. In this system we believe the bifurcated tidal morphology results from a progenitor with a warped gaseous disk (§2.2 & HY99), and we seek to understand why the inner filament is gas-poor, given that its progenitor was obviously gas-rich.

In this section we investigate a number of possible explanations for these observations. In particular, we discuss the possible role played by: differences in the initial radial distribution of the gas and stars (§3.1), dust obscuration (§3.2), kinematic decoupling of the gas due to collisions within the developing tidal tail (§3.3), ram pressure stripping of the gas, either by a halo or by a galactic scale wind (§3.4), and photoionization of the gas, either by the starburst or by local sources (§3.5).

3.1. Differences in the Radial Distribution of Gas and Starlight

In interacting systems the H I is often more widely distributed than the optical light (see, e.g. the H I map of the M81 system by Yun *et al.* 1994; see also van der Hulst 1979; Appleton, Davies & Stephenson 1981). These gas-rich extensions frequently have no associated starlight down to very faint limits (e.g. Simkin *et al.* 1986; HvG96). A natural explanation is that such features arise from the H I-rich but optically faint outer radii of the progenitor disks. The relatively short lifetimes of luminous stars and the larger velocity dispersions of less luminous stars, especially with respect to the gas, will further dilute the luminous content of this material, and the H I-to-light ratio of the resulting tidal features will increase with time (Hibbard *et al.* 1994). Gaseous tidal extensions with very little detectable starlight would seem to be the natural consequence. The outer H I rings in NGC 520 and Arp 220 and the gas-rich outer filament in Arp 299 are all likely to have arisen in

this manner.

However, gas-rich outer disks cannot give rise to gas-poor optical structures, such as the optical plume in NGC 520, the optical tail in Arp 220, or the inner filament in Arp 299. Since these features presumably arise from optically brighter regions of the progenitor disks (regions which are characterized by H I column densities higher than that of the outer disks) one would have expected a priori that these features should also be gas-rich. It is possible that the disks which gave rise to the plumes in NGC 520 and Arp 220 were gas-poor at all radii. However, this would not account for the discontinuities in the outer gaseous features that project near these optical features (i.e., NE gap in NGC 520 and NW gap in Arp 220). We therefore seek other explanations for these structures.

3.2. Effects of Dust Obscuration

The correspondence between rising gas column density and falling optical surface brightness (Fig. 4) suggests that dust associated with the cold gas may attenuate the optical light. To address this possibility, we calculate the expected extinction in the R -band for a given column density of H I. We adopt the Milky Way dust-to-gas ratio determined by Bohlin, Savage, & Drake (1978; $N_{HI}/E(B-V) = 4.8 \times 10^{21} \text{ cm}^{-2} \text{ mag}^{-1}$), which is supported by direct imaging of the cold dust in the outer regions of eight disk galaxies (Alton *et al.* 1998). This is combined with the Galactic extinction law of O’Donnell (1994; $A_R/E(B-V) = 2.673$, from Table 6 of Schlegel *et al.* 1998) to yield an expected extinction in the R -band of $A_R = \frac{N_{HI}}{1.8 \times 10^{21} \text{ cm}^{-2}} \text{ mag}$.

From Fig. 4, the peak H I column densities on either side of the optical features are $\sim 3 \times 10^{20} \text{ cm}^{-2}$. The predicted extinction is therefore of order 0.2 mag in the R -band. From Fig. 4 we see that the mean light level drops by about 1.0 mag arcsec $^{-2}$ for Arp 299 (from 26.5 mag arcsec $^{-2}$ to below 27.5 mag arcsec $^{-2}$), about 1.5 mag arcsec $^{-2}$ for NGC 520 (from 25 mag arcsec $^{-2}$ to below 26.5 mag arcsec $^{-2}$), and by about 2.5 mag arcsec $^{-2}$ for Arp 220 (from 23.5 mag arcsec $^{-2}$ to below 26 mag arcsec $^{-2}$) along the extracted slices. To produce this amount of extinction, the tidal gas would have to have a dust-to-gas ratio that is ten times that in the Milky Way.

The above analysis assumes that the measured neutral gas column density represents the total gas column density. However, the sharp drop in H I column density observed in many tidal features (HvG96, Hibbard & Yun in preparation) suggests that the tidal gas may be highly ionized by the intergalactic UV field (see also references in §3.5). Since large dust grains should survive in the presence of this ionizing radiation, the opacity per atom of neutral hydrogen (A_R/N_{HI}) should increase in regions of increasing ionization fraction. Observations of NGC 5018 (Hilker & Kissler-Patig 1996), in which blue globular clusters are absent in a region underlying an associated H I tidal stream, may support a high A_R/N_{HI} ratio for tidal gas. Nevertheless, the lack of obvious reddening of the $B - R$ colors along the slices in Arp 299 and NGC 520 (Hibbard 1995; HY99) argues against a much higher extinction in these regions.

We conclude that extinction might be important for shaping the morphology of the faintest optical features (e.g., the “Hook” and the end of the optical tail of Arp

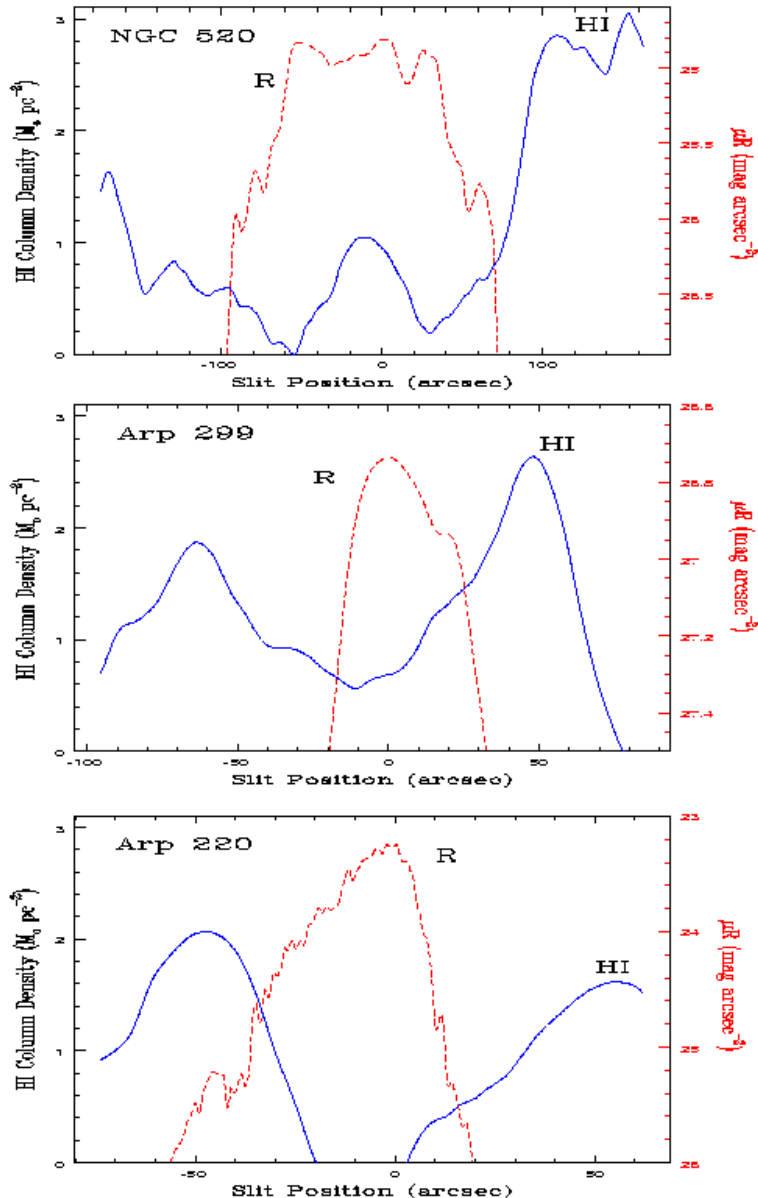


FIG. 4.— Intensity profiles of R -band surface brightness (μ_R) and HI column density (beam-averaged values measured from the low resolution data) taken along the dashed lines in Figs. 1–3. (a) (top) NGC 520, across the northern plume. (b) (middle) Arp 299, across the tip of the northern tail. (c) (bottom) Arp 220, across the NW plume. Gas column densities are measured in $M_\odot \text{pc}^{-2}$ (where $1 M_\odot \text{pc}^{-2} = 1.25 \times 10^{20} \text{cm}^{-2}$), and optical surface brightnesses in mag arcsec^{-2} .

299, Fig. 2, which has μ_R near the detection limit of 28 mag arcsec^{-2}), but is insufficient to greatly affect the overall tidal morphology. However, an anomalously high tidal dust-to-gas ratio remains a possibility. This question could be resolved by the direct detection of cold dust in tidal tails with sub-millimeter imaging.

3.3. Collisions within Developing Tidal Tails

During the tail formation process, the leading-edge of the tail is decelerated with respect to the center of mass of the progenitors, while the trailing-edge is accelerated, and the two edges move towards each other (see Toomre & Toomre 1972, Fig. 3). Eventually, the two edges appear to cross, forming a caustic (Wallin 1990; Struck-Marcell 1990). In most cases, the caustics are simply due to pro-

jection effects. Only for low-inclination encounters will these crossings correspond to physical density enhancements, and numerical experiments suggest that in these cases the density will increase by factors of a few (Wallin 1990). It has been suggested that collisions experienced by the crossing tidal streams in such low-inclination encounters may lead to a separation between the dissipational (gas) and non-dissipational (stellar) tidal components (Wevers 1984; Smith *et al.* 1997).

The present data do not allow us to directly address this question, since the kinematic decoupling presumably took place long ago. However, several arguments lead us to suspect that this collisional process is not important in tidal tails: (1) large scale decoupling between the stel-

lar and gaseous tidal morphologies is not seen in many systems known to have experienced low-inclination encounters (e.g. NGC 4038/9, “The Antennae”, Hibbard *et al.* in preparation; NGC 7252 “Atoms for Peace” Hibbard *et al.* 1994; NGC 4676 “The Mice” HvG96); (2) the broad plume-like morphologies of the optical features in Arp 220 and NGC 520 suggest rather inclined encounters (§§2.1, 2.3), in which case wide-spread collisions are not expected; and (3) the parallel filaments in the Arp 299 tail have identical kinematics, whereas one would expect kinematic differences between the stripped and unstripped material.

Therefore while gaseous collisions and dissipation might result in differences between gas and stars during tidal development (particularly along tidal bridges, where the gas streamlines are converging; e.g. Struck 1997; NGC 7714/5 Smith *et al.* 1997; Arp 295 HvG96), we believe that they are not likely to lead to a wide-spread decoupling in the outer regions.

3.4. Ram Pressure Stripping

If the tidal features pass through a diffuse warm or hot medium, or if such a medium passes through the tidal features, it is possible that the tidal gas exchanges energy and momentum with this medium due to collisions. Such effects have been proposed to explain the stripping of the cool interstellar medium from spiral galaxies as they move through the hot IGM in clusters (Gunn & Gott 1972), and is referred to as Ram Pressure Stripping (RPS). Tidal features should be relatively easily stripped, as they lack the natural restoring forces present in disk galaxies, except possibly at a small number of self-gravitating regions. In this case, the momentum imparted due to ram pressure is simply added to or subtracted from the momentum of the gaseous tidal features, and a separation of stellar and gaseous components might be expected.

In the next two subsections, we investigate two possible sources for ram pressure: an extended halo associated with the progenitors (§3.4.1); and an expanding starburst driven superwind (§3.4.2).

3.4.1. RPS from Extended Halo Gas

Our own galaxy is known to have an extended halo of hot gas (Pietz *et al.* 1998). The existence of similar halos around external galaxies has been inferred from observations of absorption line systems around bright galaxies (e.g. Lanzetta *et al.* 1995). These halos may have sufficient density to strip any low column density gas moving through them. Several investigators have suggested that such stripping is responsible for removing gas from the Magellanic Clouds as they orbit through the Galaxy’s halo, producing the purely gaseous Magellanic Stream (e.g. Meurer, Bicknell & Gingold 1985; Sofue 1994; Moore & Davis 1994). Sofue & Wakamatsu (1993) and Sofue (1994) specifically stress that stripping by galaxy halos should also play an important role in the evolution of H I tidal tails.

The tidal features in each of our systems have H I column densities and velocities similar to those assumed in the numerical models of Sofue (1994) and Moore & Davis (1994), which resulted in rather extreme stripping of the H I clouds. Although this may seem to provide an immediate explanation for our observations of gas/star dis-

placements, we point out that these column densities and velocities are typical of all of the tails thus far imaged in H I, the great majority of which do not show the extreme displacements we describe here. There is no reason to believe that the halo properties of NGC 520, Arp 299 and Arp 220 are any different from, or that the encounters were any more violent than similar mergers which do not exhibit such dramatic displacements (e.g., NGC 4038/9, NGC 7252, NGC 4676 HvG96; NGC 3628 Dahlem *et al.* 1996; NGC 2623, NGC 1614, Mrk 273 Hibbard & Yun in preparation; NGC 3256 English *et al.* 1999). In fact, in light of the stripping simulations mentioned above, one wonders why such displacements are not more common.

A possible solution to this puzzle is suggested by the results of numerical simulations of major mergers. In these simulations, the material distributed throughout the halos of the progenitors is tidally distended along with the tails, forming a broad sheath around them (see e.g. the video accompanying Barnes 1992). This sheath has similar kinematics as the colder tail material, resulting in much lower relative velocities than if the tail was moving through a static halo, thereby greatly reducing any relative ram pressure force.

In summary, while halo stripping might be effective for discrete systems moving through a static halo (such as the LMC/SMC through the halo of the Galaxy, or disks through a hot cluster IGM), the lack of widespread H I/optical decoupling in mergers suggests that it is not very effective for removing gas from tidal tails, and it does not appear to be a suitable explanation of the present observations.

3.4.2. RPS from Expanding Superwind

The three systems under discussion host massive nuclear starbursts with associated powerful outflows or “superwinds”. Optical emission lines and/or X-ray emission reveal that the observed outflows extend for tens of kpc from the nuclear regions. Theoretical calculations suggest that the observed gas plumes represent just the hottest, densest regions of a much more extensive, lower density medium (Wang 1995). In each of these three systems, the most extreme gaps in the H I distribution appear along the inferred direction of the expanding hot superwind (Figs. 1d, 2d, 3d). A very similar anti-correlation between an outflowing wind and tidally disrupted H I has been observed in the M82 system (Yun *et al.* 1993; Strickland *et al.* 1997; Shopbell & Bland-Hawthorn 1998), the NGC 4631 system (Weliachew *et al.* 1978; Donahue *et al.* 1995; Wang *et al.* 1995; Vogler & Pietsch 1996), and possibly the NGC 3073/9 system (Irwin *et al.* 1987; Filippenko & Sargent 1992). It has been suggested that this anti-correlation is due to an interaction between the blown-out gas of the superwind and the cold gaseous tidal debris, either as the wind expands outward into the debris, or as the tidal debris passes through the wind (Chevalier & Clegg 1985; Heckman, Armus & Miley 1987, and references above).

Figure 5 presents the suggested geometry for the case of Arp 299. This figure is constructed from our preliminary efforts to model the northern tail of Arp 299 using N-body simulations similar to those presented in Hibbard & Mihos (1995; i.e. no hydrodynamical effects are included). We found that we could not match the morphology and kinematics of both filaments simultaneously, but could match

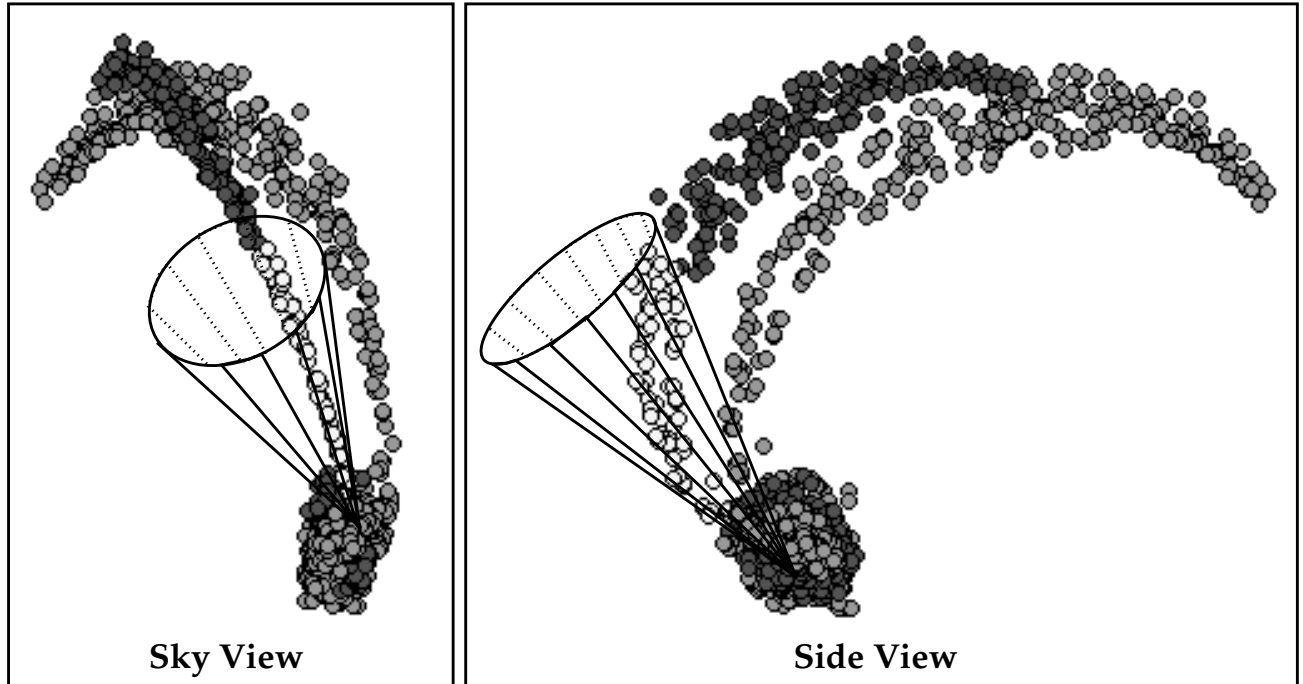


FIG. 5.— An illustration of the proposed relative placement of the tidal tail and the expanding wind or ionization cone for the case of Arp 299. In this figure, the purely gaseous tidal filament is represented by light grey circles, whereas the optical tidal filament is represented by circles drawn with two shades: regions of the optical tail which have accompanying H I are shaded dark grey, while the regions which have been cleared of H I are shaded white (see Fig. 2). The suggested geometry of the superwind bubble (cf. §3.4.2) or ionization cone (cf. §3.5.1) is indicated by the cone, which has been drawn to encompass the white circles in the optical filament. This figure illustrates how the restricted opening angle of such a cone may only intersect a portion of the ribbon-like tail.

either one separately. Fig. 5 presents the results of combining these two solutions. In this sense this figure is *not a self-consistent fit to the data*, but simply a cartoon which illustrates the proposed relative placement of the tidal tail and the expanding wind. In this figure, the wind opening angle is illustrated by the cone, the gas-rich regions of the tails are represented by dark and light grey circles, and the gas-poor regions of the tails are represented by white circles. The figure illustrates how the restricted opening angle of such a wind (or of an ionization cone, cf. §3.5.1) may intersect only a portion of the ribbon-like tail.

Here we estimate whether ram pressure stripping by the nuclear superwind can exert sufficient pressure on gas at the large distances typical of tidal tails. We use equation (5) from Heckman, Lehnert & Armus (1993; see also Chevalier & Clegg 1985) to calculate the expected ram pressure (P_{RPS}) of the superwind far from the starburst as a function of its bolometric luminosity (L_{bol}):

$$P_{RPS}(r) = 4 \times 10^{-10} \text{ dyne cm}^{-2} \left(\frac{L_{bol}}{10^{11} L_{\odot}} \right) \left(\frac{1 \text{ kpc}}{r} \right)^2 \quad (1)$$

This equation has been shown to fit the pressure profile derived from X-ray and optical emission line data of Arp 299 (Heckman *et al.* 1999). It should provide a lower

limit to the ram pressure, since it assumes that the wind expands spherically, while observations suggest that the winds are limited in solid angle.

This pressure can be compared with the pressure of the ambient medium in the tidal tail (P_{tidal}), given by the energy per unit volume:

$$P_{tidal} = C \times \rho_{gas} \sigma_{gas}^2 \quad (2)$$

where C is a constant, ρ_{gas} is the mass density of the gas, and σ_{gas} is the velocity dispersion of the gas. For an equation of state of the form $P \sim \rho^\gamma$, the constant C is equal to $\gamma^{-1} = \frac{3}{5}$, and σ_{gas} corresponds to gas sound speed, while for a self-gravitating cloud, $C = \frac{3}{2}$ and σ_{gas} is the one-dimensional velocity dispersion of the cloud. In both cases, we assume that the observed line-of-sight velocity dispersion of the H I is a suitable measure of σ_{gas} .

The mass density of the tidal gas is given by $\rho_{gas} = 1.36 \times m_H \times n_{HI}$, where the numerical constant accounts for the presence of He, m_H is the mass of a hydrogen atom, and n_{HI} is the number density of atomic hydrogen. If we assume the gas is uniformly distributed⁶ with a column density N_{HI} along a length dL , we have $n_{HI} = 6.5 \times 10^{-3} \text{ cm}^{-3} \left(\frac{N_{HI}}{2 \times 10^{20} \text{ cm}^{-2}} \right) \left(\frac{10 \text{ kpc}}{dL} \right)$, where the fiducial values are typical of tidal features (HvG96, Hib-

⁶Clearly the results will be very different if the tidal gas is mainly in dense clouds, a point that can be tested with higher-resolution VLA observations. For now we calculate the ram pressure effect on the diffuse gas.

bard & Yun in preparation). We rewrite eqn. (2) in terms of the observables:

$$P_{tidal} = 2 \times 10^{-14} \text{ dyne cm}^{-2} \left(\frac{C}{1.5} \right) \left(\frac{N_{HI}}{2 \times 10^{20} \text{ cm}^{-2}} \right) \left(\frac{10 \text{ kpc}}{dL} \right) \left(\frac{\sigma_{HI}}{10 \text{ km s}^{-1}} \right)^2 \quad (3)$$

The maximum radius out to which we expect material to be stripped (R_{RPS}) is then given by the requirement that $P_{RPS}(r) = P_{tidal}(r)$ at $r = R_{RPS}$. We replace L_{bol} in eqn. (1) by the IR luminosity (L_{IR}), under the assumption that the IR luminosity arises from reprocessed UV photons from the starburst⁷ (Lonsdale, Persson & Matthews 1984, Joseph & Wright 1985). The very high IR luminosities of these systems ($L_{IR}/L_B > 10$) make it likely that this is indeed the case, and we are probably making an error of $\lesssim 10\%$ (e.g. Heckman, Lehnert & Armus 1993). Equating eqns. (1) and (3) we find:

$$R_{RPS} = 140 \text{ kpc} \left(\frac{1.5}{C} \right)^{\frac{1}{2}} \left(\frac{L_{IR}}{10^{11} L_{\odot}} \right)^{\frac{1}{2}} \left(\frac{2 \times 10^{20} \text{ cm}^{-2}}{N_{HI}} \right)^{\frac{1}{2}} \left(\frac{dL}{10 \text{ kpc}} \right)^{\frac{1}{2}} \left(\frac{10 \text{ km s}^{-1}}{\sigma_{HI}} \right) \quad (4)$$

In Table 1 we provide estimates of R_{RPS} for the systems considered here. In calculating R_{RPS} we made the very conservative assumption that the values of N_{HI} and σ_{HI} for the stripped gas are equal to the maximum values found within the tidal tails (see Table 1). The results of these calculations indicate that, in all cases, R_{RPS} is larger than the radii of the observed gaps in the tidal H I distributions. Therefore, in principle, the wind should be able to strip the gas from any tidal material in its path.

The above derivation assumes that the tidal gas is at rest with respect to the wind. It can be easily generalized to the case of a wind impacting an expanding tidal feature by reducing the wind ram pressure by a factor $\left(\frac{V_{wind} - V_{tidal}}{V_{wind}} \right)^2$. For NGC 520 and Arp 220, the tidal gas is primarily in rotation (*i.e.*, moves perpendicular to superwind), so we expect the gas to feel the full ram pressure given above. For Arp 299, Heckman *et al.* (1999) find $V_{wind} = 800 \text{ km s}^{-1}$, and we estimate a maximum $V_{tidal} = 240 \text{ km s}^{-1}$ (HY99). Therefore, the ram pressure could be reduced by 50%, reducing R_{RPS} by 70% from that listed in Table 1, *i.e.* $R_{RPS} \sim 100 \text{ kpc}$ for Arp 299. This is still large enough to reach to the region of the N clump in Fig. 2. The regions of high H I velocity dispersion indicated in Fig. 2c may be due to the influence of such a wind. We note that these regions occur on the side of the H I features that face the starburst region. However, no such kinematic signatures are visible in the gas near the wind axis in NGC 520 or Arp 220.

The lack of gaseous/stellar displacements in the tidal tails of many superwind systems might seem to provide a strong argument against the scenario outlined above. However, there are two conditions needed to produce wind-displaced tidal features: the starburst must be of sufficient

energy and duration to achieve “blowout”, and the tidal H I must intersect the path of the expanding wind material. The second condition is not met for the blowout systems NGC 4676, NGC 3628, NGC 2623, NGC 1614, and NGC 3256 (references given in §3.4.1). In these systems the tidal tails appear to lie at large angles with respect to the blowout axis, and their tidal tails should not intersect the wind. Both conditions are met for M82 and NGC 4631, which both show extreme H I/optical displacements. For these two systems, the high-latitude H I appears to be accreted from nearby disturbed companions (M81 and NGC 4656, respectively; Yun *et al.* 1993, Wellichew *et al.* 1978), while for the three major mergers under study here the H I appears to intercept the path of the wind as a result of a highly inclined encounter geometry. A high inclination encounter geometry is therefore a prerequisite for such displaced morphologies, and the host of the superwind should be the disk with a retrograde or polar spin geometry.

Nevertheless, ram pressure stripping cannot provide a complete explanation of the observations. Since the stars are unaffected by the wind, it would be an unusual coincidence for the edges of the optical plumes to correspond with the edge of the cold gas which is presently being ablated. Nor does it seem likely that the wind could be sufficiently collimated to “bore” into the northern H I clump in Arp 299 just where the optical tail appears projected upon it. Therefore a second process is still needed to explain the small-scale anti-correlations. In conclusion, the expanding wind *should* affect any tidal H I in its path; however this effect alone cannot explain all the details of the observations.

3.5. Photoionization

Disk galaxies are known to exhibit a precipitous drop in neutral hydrogen column density beyond column densities of a few times 10^{19} cm^{-2} (Corbelli, Schneider & Salpeter 1989; van Gorkom 1993; Hoffman *et al.* 1993). This drop has been attributed to a rapid change in the ionization fraction of the gas due to influence of the intergalactic UV field (Maloney 1993, Corbelli & Salpeter 1993, Dove & Shull 1994; see also Felten & Bergeron 1969, Hill 1974), rather than a change in the total column density of H.

Tidal tails are assembled from the outermost regions of disk galaxies. Since this material is redistributed over a much larger area than it formerly occupied, its surface brightness must decrease accordingly. Therefore, if the progenitors were typical spirals, with H I disks extending to column densities of a few times 10^{19} cm^{-2} , then the resulting tidal tail *must* have gas at much lower column densities. However, tidal tails exhibit a similar edge in their column density distribution *at a similar column density* (HvG96; Hibbard & Yun in preparation). This is one of the most compelling pieces of evidence for an abrupt change in the phase of the gas at low H I column density. The outer tails mapped in H I should therefore be the proverbial “tip of the iceberg” of a lower column density, mostly ionized medium. With the tidal gas in this very diffuse state, fluctuations in the incident ionizing flux

⁷This assumes that the IR luminosity is not enhanced due to the presence of AGN. There is no evidence for an energetically important AGN in any of these three systems.

might be expected to produce accompanying fluctuations in the neutral gas fraction.

Given these considerations, we examine the possibility that the total hydrogen column density does not change at the regions illustrated in Figs. 1–4, but that the neutral fraction does, *i.e.* that the gas in the regions under study has a higher ionization fraction than adjacent regions. The intergalactic UV field should be isotropic, and would not selectively ionize certain regions of the tails. Here we examine the possibility of two non-isotropic sources of ionizing flux: (1) leakage of UV flux from the circumnuclear starburst; (2) ionization by late B stars and white dwarfs associated with the evolved stellar tidal population.

Our procedure is to compare the expected ionizing flux density shortward of 912 Å to the expected surface recombination rate of the gas. We assume that in the area of interest the gas is at a temperature of $\sim 10^4$ K, for which a case-B recombination coefficient of $\alpha_B = 2.6 \times 10^{-13} \text{ cm}^3 \text{ s}^{-1}$ is appropriate (Spitzer 1956). We assume that the hydrogen is almost completely ionized, so $n_e \approx n_H$. We further assume that the density of ionized gas is the same as the density of the neutral gas in the adjacent regions, $n_H \approx n_{HI}$, where n_{HI} is calculated as above ($n_H \sim N_{HI}/dL$, §3.4.2). The detailed ionization state will depend sensitively on the clumpiness of the gas, but a full treatment of this problem is beyond the scope of this paper. Here we wish to investigate if these processes are in principle able to create effects similar to those observed.

3.5.1. Photoionization by the Starburst

Here we consider the case that the superwind does not affect the tidal gas by a direct interaction, but influences it by providing a direct path from the tidal regions to the starburst, free of dust and dense gas (see also Fig. 5). Through these holes, ionizing photons from the young hot stars stream out of the nuclear regions and are quickly absorbed by the first neutral atoms they encounter. Following Felton & Bergeron (1969; see also Mahoney 1993), we solve the equation:

$$n_{HI}^2 \alpha_B dL = I = \frac{1}{4\pi r^2} \int_{h\nu=13.6\text{eV}}^{\infty} \frac{L_\nu}{h\nu} d\nu \quad (5)$$

The right hand side of this equation represents the total ionizing radiation escaping the starburst region along a direction that has been cleared of obscuring material by the superwind. We express this in terms of the total ionizing flux of a completely unobscured starburst of a given bolometric luminosity L_{bol} by introducing the factor $f_{esc}(\Omega_{wind})$ to account for the fact that only a fraction of the photons emitted into a solid angle Ω_{wind} find their way out of the starburst region⁸. The expected ionizing flux for a starburst of a given bolometric luminosity L_{bol} is calculated from the population synthesis models of Bruzual & Charlot (1993; 1995), assuming continuous star formation with a duration longer than 10 Myr (long enough for the burst to achieve blowout), a Salpeter IMF with $M_{lower} =$

$0.1M_\odot$ and $M_{upper} = 125M_\odot$, and solar metallicity. This yields⁹ $I = f_{esc}(\Omega_{wind}) \times \frac{1.83 \times 10^{54} \text{ photons s}^{-1}}{4\pi r^2} \times \frac{L_{bol}}{10^{11} L_\odot}$. Again making the standard assumption that most of the starburst luminosity is emitted in the far infrared (*i.e.* $L_{bol} = L_{IR}$, cf. §3.4.2), we rearrange eqn. (5) to solve for the radius, $R_{ionized}$, out to which the starburst is expected to ionize a given column density of H I of thickness dL :

$$R_{ionized} = 66 \text{ kpc} \left(\frac{f_{esc}(\Omega_{wind})}{0.10} \right)^{1/2} \left(\frac{L_{IR}}{10^{11} L_\odot} \right)^{1/2} \left(\frac{2 \times 10^{20} \text{ cm}^{-2}}{N_{HI}} \right) \left(\frac{dL}{10 \text{ kpc}} \right)^{1/2} \quad (6)$$

Resulting values for $R_{ionized}$ are listed in Table 1. For this computation, we have adopted a value of 10% for $f_{esc}(\Omega_{wind})$. This is equal to the total fraction of ionizing photons, f_{esc} , escaping from a normal disk galaxy as calculated by Dove, Shull & Ferrara (1999). Even higher values of f_{esc} are expected in starburst systems (Dove *et al.* 1999). Since we stipulate that a higher fraction of ionizing photons escape along sightlines above the blowout regions than are emitted along other directions, it follows that $f_{esc}(\Omega_{wind}) > f_{esc}$, and as a result the values of $R_{ionized}$ calculated in Table 1 should be conservative estimates.

Table 1 shows that under these simplified conditions, $R_{ionized}$ is of the order of, or larger than, the tidal radii of interest. We therefore conclude that the starburst seems quite capable of ionizing tidal H I, if indeed there is an unobstructed path from the starburst to the tidal regions. This might explain the lack of H I along the wind axis in NGC 520 and Arp 220, and the absence of H I along the optical tidal tail in Arp 299.

This process is especially attractive since it can potentially explain the lack of H I at the bases of otherwise gas-rich tidal tails in NGC 7252 (Hibbard *et al.* 1994), Arp 105 (Duc *et al.* 1997), and NGC 4039 (Hibbard, van der Hulst & Barnes in preparation). These systems do *not* show evidence for expanding superwinds, which rules out the possibility that RPS is playing a role. And each of these systems possesses a level of star formation that, according to eqn. 6, is capable of ionizing gas out to the necessary radii.

However, photoionization by the central starburst does not seem capable of explaining all of the observations. As with the wind hypothesis above, it would be an unusual coincidence for the edges of the optical plumes to correspond with the edge of ionization cone. Therefore a second process is still needed to explain the small-scale anti-correlations.

3.5.2. Photoionization by the Optical Tails

The fact that the H I column density falls off just as the optical surface brightness increases at the edges of various tidal features (Fig. 4) leads us to suspect that there may be local sources of ionization within the stellar features themselves. For NGC 520 and Arp 220, we believe the outer H I

⁸It is important to differentiate f_{esc} , the total fraction of ionized photons emerging from a starburst, and $f_{esc}(\Omega_{wind})$, the fraction emerging along a particular sightline. f_{esc} is the total angle averaged fraction, *i.e.* f_{esc} is the integral of $f_{esc}(d\Omega)$ over all solid angles, while $f_{esc}(\Omega_{wind})$ is the integral over a solid angle cleared by the wind. Most studies in the literature quote values for f_{esc} .

⁹With similar assumptions, the ‘‘Starburst99’’ models of Leitherer *et al.* (1999) give approximately the same numerical coefficient.

is in a disk structure which is intersected by the tidal stellar plumes and we wish to investigate whether ionization by evolved sources within the stellar plumes, such as late B stars and white dwarfs, could be responsible for decreasing the neutral fraction of the diffuse outer H I. For Arp 299 the geometry is more complicated, and we refer the reader to Fig. 5. Here we suggest that part of the purely gaseous tidal filament (the light grey filament in Fig. 5) is ionized by evolved sources near the end of the stellar tail (the dark grey filament in Fig. 5, especially those regions nearest the gas-rich filament in the right hand panel of this figure).

As in the previous section, we balance the surface recombination rate with the expected ionizing flux density (eqn. 5). In this case, we calculate the ionizing flux density for an evolved population of stars of a given R -band luminosity density (Σ_R , in $L_\odot \text{pc}^{-2}$).

In order to approximate the stellar populations in the tidal tails, we assume that the tails arise from the outer edges of an Sbc progenitor, and that star formation ceased shortly after the tails were launched. We again use the models of Bruzual & Charlot (1993, 1995) for a Salpeter IMF over the mass range 0.1–125 M_\odot , and adopt an exponentially decreasing SFR with a time constant of 4 Gyr (typical of an Sbc galaxy, Bruzual & Charlot 1993), which is truncated after 10 Gyr and allowed to age another 500 Myr. This simulates the situation in which star formation within the disk is extinguished as the tail forms, and the ejected stellar population passively fades thereafter. While tidal tails frequently exhibit *in-situ* star formation (e.g. Schweizer 1978; Mirabel, Lutz & Maza 1991), it is usually not widespread. Under these assumptions, a population with a projected R -band surface brightness of 1 $L_{R,\odot} \text{pc}^{-2}$ should produce an ionizing flux of $2.36 \times 10^4 \text{ph s}^{-1} \text{cm}^{-2}$. Therefore eqn. (5) becomes $n_{\text{HI}}^2 \alpha_B dL < 2.36 \times 10^4 \text{ph s}^{-1} \text{cm}^{-2} \times \Sigma_R$, which can be rewritten as:

$$\Sigma_R > 14.28 L_{R,\odot} \text{pc}^{-2} \left(\frac{N_{\text{HI}}}{2 \times 10^{20} \text{cm}^{-2}} \right)^2 \left(\frac{10 \text{kpc}}{dL} \right) \quad (7)$$

Noting that 1 $L_\odot \text{pc}^{-2}$ corresponds to $\mu_R = 25.9 \text{mag arcsec}^{-2}$, we rewrite this as a condition on the surface brightness of the tidal features:

$$\mu_R < 23.0 \text{mag arcsec}^{-2} - 2.5 \times \log \left[\left(\frac{N_{\text{HI}}}{2 \times 10^{20} \text{cm}^{-2}} \right)^2 \left(\frac{10 \text{kpc}}{dL} \right) \right] \quad (8)$$

Referring to Fig. 4, we see that only the northern plume of Arp 220 is bright enough to ionize nearby tidal H I at the appropriate column densities. Neither the optical plume in the NGC 520 system nor the northern tail in the Arp 299 system appears bright enough to ionize the necessary columns of hydrogen unless the tidal features are unreasonably thick ($\sim 60 \text{kpc}$). However, since we have no other explanation for the small scale H I/optical differences illustrated in Fig. 4, we are hesitant to abandon this explanation too quickly.

A possible solution is to invoke continued star formation even after the tails are ejected. For instance, if we

do not truncate the star formation rate after 10 Gyr, instead allowing the star formation rate to continue its exponential decline as the tail expands, then the ionizing flux per 1 $L_{R,\odot} \text{pc}^{-2}$ is 70 times higher than the value of $2.36 \times 10^4 \text{ph s}^{-1} \text{cm}^{-2}$ used above. This would lower the fiducial surface brightness in eqn. (8) from 23.0 mag arcsec^{-2} to 27.5 mag arcsec^{-2} , in which case the faint tidal features in NGC 520 ($\mu_R \sim 25 \text{mag arcsec}^{-2}$) and Arp 299 ($\mu_R \sim 26.5 \text{mag arcsec}^{-2}$) could indeed ionize the necessary column densities of adjoining H I.

The observed broad-band colors of the tidal tails are not of sufficient quality to discriminate between these two star formation histories, since the expected color differences are only of order $B - R = 0.1 \text{mag}$. However, whether or not the gas is more highly ionized in the regions of interest can be addressed observationally. The expected emission measure ($EM = \int n_e^2 dl$) can be parameterized as:

$$EM = 0.42 \text{cm}^{-6} \text{pc} \left(\frac{N_{\text{HI}}}{2 \times 10^{20} \text{cm}^{-2}} \right)^2 \left(\frac{10 \text{kpc}}{dL} \right)^2 \quad (9)$$

Since emission measures of order $0.2 \text{cm}^{-6} \text{pc}$ have been detected with modern CCD detectors (e.g. Donahue *et al.* 1995; Hoopes, Walterbos & Rand 1999), there is some hope of being able to observationally determine if regions of the tidal tails are significantly ionized. If the gas has a clumpy distribution, then there should be some high density peaks which might be sufficiently bright to yield reliable emission line ratios. Such ratios would allow one to determine the nature of the ionizing source, e.g. photoionization vs. shocks. Therefore, while we cannot assert unequivocally that photoionization plays a role in shaping the outer tidal morphologies, it is possible to test this hypothesis with future observations.

The hypothesis that ionizing flux from a stellar tidal feature may ionize gas in a nearby gaseous tidal feature is not necessarily at odds with the observations that many stellar tails are gas-rich. This is because tails with cospatial gas and stars arise from regions originally located within the stellar disk of the progenitors, while the optical faint gas-rich tidal features likely arise from regions beyond the optical disk (§ 3.1). In normal disk galaxies, the H I within the optical disk is dominated by a cooler component with a smaller scale height and velocity dispersion, while the H I beyond the optical disk is warmer and more diffuse, with a larger scale height and velocity dispersion (Braun 1995, 1997). As a result, dL should be considerably larger for purely gaseous tidal features than for optically bright tidal features.

4. CONCLUSIONS

In this paper we have described differences between gaseous and stellar tidal features. There are large-scale differences, such as extensive purely gaseous tidal features (the outer disks in NGC 520 and Arp 220 and the outer filament in Arp 299) and largely gas-poor optical features (tidal plumes in NGC 520 and Arp 220 and the inner filament in Arp 299). And there are smaller-scale differences: the anti-correlation between the edges of gaseous and optical features depicted in Fig. 4. A similar anti-correlation

is observed between HI and optical shells in shell galaxies (Schiminovich *et al.* 1994a,b, 1999), many of which are believed to be more evolved merger remnants.

We have examined a number of possible explanations for these observations, including dust obscuration, differences in the original distribution of gas and starlight in the progenitor disks, gas cloud collisions within the developing tails, ram pressure stripping due to an extensive hot halo or an expanding superwind, and photoionization by either the central starburst or evolved sources in the tidal tails themselves. However, no one model easily and completely explains the observations, and it is conceivable that all explanations are playing a role at some level.

The most likely explanation for the lack of starlight associated with the outer tidal HI is that such features arise from the HI-rich but optically faint outer radii of the progenitor disks. The relatively short lifetimes of luminous stars and the large velocity dispersions of less luminous stars, especially with respect to the gas, will further dilute the luminous content of this material, and the HI-to-light ratio of the resulting tidal features will increase with time (Hibbard *et al.* 1994). Gaseous tidal extensions with very little detectable starlight would seem to be the natural consequence. The outer HI rings in NGC 520 and Arp 220 and the gas-rich outer filament in Arp 299 are all likely to arise from these gas-rich regions of their progenitor disks.

For the gas-poor tidal features we suggest that the starburst has played an important role in shaping the gaseous morphology, either by sweeping the features clear of gas via a high-pressure expanding superwind, or by excavating a clear sightline towards the starburst and allowing ionizing photons to penetrate the tidal regions. The primary supporting evidence for this conclusion is rather circumstantial: the five galaxies with the most striking HI/optical displacements (the three systems currently under study here, and the HI accreting starburst systems M82 and NGC 4631) host massive nuclear starbursts with associated powerful outflows or superwinds aligned with the direction of the most extreme HI/optical displacements.

NGC 520, Arp 299, and Arp 220 each experienced prograde/polar or prograde/retrograde encounters. This relative geometry may be a pre-requisite for the morphological differences reported here. Retrograde and polar encounters do not raise extensive tidal tails (e.g. Barnes 1988), leaving large gaseous disks in the inner regions. These disks should help collimate and “mass-load” the superwind (Heckman, Lehnert & Armus 1993; Suchkov *et al.* 1996), which in turn leads to denser and longer-lived winds. Simultaneously, the combination of opposite spin geometries provides the opportunity for the tidal tail from the prograde system to rise above the starburst region in the polar or retrograde system, where it may intersect the escaping superwind or UV radiation. If this suggestion is correct, only systems hosting a galactic superwind and experiencing a high-inclination encounter geometry should exhibit such extreme differences between their HI and optical tidal morphologies.

The observations do not allow us to discriminate between either the RPS or the photoionization models: sim-

ple calculations suggest that either is capable of affecting the diffuse outer gas if the geometry is right. There might be some evidence for the effects of an impinging wind on the outer material in Arp 299 from the increased velocity dispersion at several points (HY99); however NGC 520 and Arp 220 show no such signatures. Photoionization is an attractive solution, as it offers a means of explaining the lack of tidal HI found at the base of otherwise gas-rich tidal tails in mergers which show no evidence of a superwind (e.g. NGC 7252, Arp 105, NGC 4039; see § 3.5.1).

Since any ionized hydrogen will emit recombination lines, both explanations can be checked observationally. The expected emission measure is given by eqn. (9), which predicts detectable features at the column densities of interest. The morphology of the ionized gas should reveal the nature of the ionizing source: photoionized gas should be smoothly distributed, while gas excited by RPS should be concentrated in dense shocked regions on the edges of the HI that are being compressed by the superwind, *i.e.* on the edges nearest the wind axis in Figs. 1d, 2d & 3d. If the gas is clumpy, there may be regions bright enough to allow line ratios to be measured, which should further aid in discriminating between photoionization or shock excitation.

Only two scenarios are offered to explain the small-scale anti-correlations: dust obscuration and photoionization due to evolved sources in the optical tails. Dust obscuration likely affects the apparent tidal morphologies at the lowest light levels, but we suspect that the dust content is too low to significantly obscure the brighter tidal features. However, if the tidal tails are highly ionized, with the neutral gas representing only a small fraction of the total hydrogen column density, it is possible that we are grossly underestimating the expected amount of absorption. This question can be investigated directly with submm imaging of the cold dust in tidal tails.

The other possibility is that the UV flux from evolved sources in the optical tails is responsible for ionizing nearby diffuse outer HI. A simple calculation suggests that the tidal tail in Arp 220 is bright enough to ionize nearby HI, but the expected ionization flux from the optical tails in NGC 520 and Arp 299 is too low to explain the observed differences, unless significant star formation continued within these features after their tidal ejection. If this is indeed the case, then the regions where the neutral gas column density drops rapidly (see Fig.4) should contain ionized gas which would emit recombination radiation. The expected levels of emission should be observable with deep imaging techniques (see above). This situation requires that the gas and stellar features are physically close, and not just close in projection, which can be tested with detailed numerical simulations.

We would like to thank Lee Armus, Tim Heckman for sharing of unpublished results, and Rhodri Evans, Jacqueline van Gorkom, Dave Schiminovich, and Josh Barnes for useful discussions. We thank the referee, Chris Mihos, for a thorough and useful report.

REFERENCES

- Aaronson, M. Huchra, J., Mould, J., Schechter, P. L. & Tully, R. B. 1982, *ApJ*, 258, 64
- Alton, P. B., Trewhella, M., Davies, J. I., Evans, R., Bianchi, S., Gear, W., Thronson, H., Valentijn, E. & Witt, A. 1998, *A&A*, 335, 807
- Appleton, P. N., Charmandaris, V. & Struck, C. 1996, *ApJ*, 468, 532
- Appleton, P. N., Davies, R. D. & Stephenson, R. J. 1981, *MNRAS*, 195, 327
- Appleton, P. N., Ghigo, F. D., van Gorkom, J. H., Schombert, J. M., & Struck-Marcell, C. 1987, *Nature*, 330, 140
- Armus, L., Heckman, T. M., & Miley, G. K. 1990, *ApJ*, 364, 471
- Barnes, J. E. 1988, *ApJ*, 331, 699
- Barnes, J. E. 1992, *ApJ*, 393, 484
- Barnes, J. E. & Hernquist, L. 1991, *ApJ*, 370, L65
- Barnes, J. E. & Hernquist, L. 1996, *ApJ*, 471, 115
- Bohlin, R. C., Savage, B. D. & Drake, J. F. 1978, *ApJ*, 224, 132
- Braun, R. 1995, *A&AS*, 114, 409
- Braun, R. 1997, *ApJ*, 484, 637
- Bruzual, A. G. & Charlot, S. 1993, *ApJ*, 405, 538
- Bruzual, A. G. & Charlot, S. 1995, personal communication
- Chevalier, R. A. & Clegg A. W. 1985, *Nature*, 317, 44
- Combes, F. 1978, *A&A*, 65, 47
- Combes, F., Dupraz, C., Casoli, F., & Pagani, L. 1988, *A&A (Lett.)*, 203, 9
- Condon, J. J., Helou, G., Sanders, D. B., & Soifer, B. T. 1990, *ApJS*, 73, 359
- Corbelli, E. & Salpeter, E. E. 1993, *ApJ*, 419, 104
- Corbelli, E., Schneider, S. E. & Salpeter, E. E. 1989, *AJ*, 97, 390
- Dahlem, M., Heckman, T. M., Fabbiano, G., Lehnert, M. D., & Gilmore, D. 1996, *ApJ*, 461, 724
- Donahue, M., Aldering, G., & Stocke, J. T. 1995, *ApJ (Lett.)*, 450, L45
- Dove, J. B. & Shull, J. M. 1994, *ApJ*, 423, 196
- Dove, J. B. & Shull, J. M. & Ferrara 1999, *ApJ*, in press (astro-ph/9903331)
- Downes, D. & Solomon, P. M. 1998, *ApJ*, 507, 615
- Duc, P. -A., Brinks, E., Wink, J. E., & Mirabel, I. F. 1997, *A&A*, 326, 537
- English, J. *et al.* 1999, *AJ*, submitted
- Felton, J. E. & Bergeron, J. 1969, *ApJL*, 4, 155
- Filippenko, A. V. & Sargent, W. L. W. 1992, *AJ*, 103, 28
- Gardiner, L. T. & Noguchi, M. 1996, *MNRAS*, 278, 191
- Gunn, J. E. & Gott, J. R. 1972, *ApJ*, 176, 1
- Heckman, T. M., Armus, L., Miley, G. K. 1987, *AJ*, 93, 276
- Heckman, T. M., Armus, L., Miley, G. K. 1990, *ApJS*, 74, 833 (**HAM90**)
- Heckman, T. M., Armus, L., Weaver, K. A. & Wang, J. 1999, *ApJ*, 517, 130
- Heckman, T. M., Dahlem, M., Eales, S. A., Fabbiano, G., & Weaver, K. 1996, *ApJ*, 457, 616
- Heckman, T. M., Lehnert, M. & Armus, L. 1993, in "The Evolution of Galaxies and their Environment", edited by H. A. Thronson and J. M. Shull (Kluwer, Dordrecht), p. 455
- Hibbard, J. E. 1995, Ph. D. Thesis, Columbia University
- Hibbard, J. E. & van Gorkom, J. H. 1996, *AJ*, 111, 655 (**HvG96**)
- Hibbard, J. E., Guhathakurta, P., van Gorkom, J. H., & Schweizer, F. 1994, *AJ*, 107, 67
- Hibbard, J. E. & Mihos, J. C. 1995, *AJ*, 110, 140
- Hibbard, J. E. & Yun, M. S. 1996, in "Cold Gas at High Redshift", edited by M. Bremer, H. Rottgering, P. van der Werf, and C. L. Carilli (Kluwer, Dordrecht), p. 47
- Hibbard, J. E. & Yun, M. S. 1999, *AJ*, 118, 162 (**HY99**)
- Hilker, M. & Kissler-Patig, M. 1996, *A&A*, 314, 357
- Hill, J. K. 1974, *A&A*, 34, 431
- Hoffman, L. G., Lu, N. Y., Salpeter, E. E., Farhat, B., Lamphier, C. & Roos, T. 1993, *AJ*, 106, 39
- Hoopes, C., Walterbos, R. & Rand, R. 1999, *ApJ*, 522, 669
- van der Hulst, J. M. 1979, *A&A*, 75, 97
- Irwin, J. A., Seaquist, E. R., Taylor, A. R. & Duric, N. 1987, *ApJ (Lett.)*, 313, L91
- Joseph, R. D. & Wright, G. S. 1985, *MNRAS*, 214, 87
- Lanzetta, K. M., Bowen, D. V., Tytler, D. & Webb, J. K. 1995, *ApJ*, 442, 538
- Lehnert, M. D. & Heckman, T. M. 1996, *ApJ*, 462, 651
- Lonsdale, C. J., Persson, S. E., & Matthews, K. 1984, *ApJ*, 287, 95
- Maloney, P. 1993, *ApJ*, 414, 41
- Meurer, G. R., Bicknell, G. V. & Gingold, R. A. 1985, *PASA*, 6, 195
- Mihos, J. C. 2000, in preparation
- Mihos, J. C. & Bothun, G. D. 1998, *ApJ*, 500, 619
- Mihos, J. C., Bothun, G. D., Richstone, D. O. 1993, *ApJ*, 418, 82
- Mihos, J. C. & Hernquist, L. 1996, *ApJ*, 464, 641
- Mirabel, I. F., Lutz, D. & Maza, J. 1991, *A&A*, 243, 367
- Moore, B. & Davis, M. 1994, *MNRAS*, 270, 209
- Noguchi, M. 1988, *A&A*, 201, 37
- Nordgren, T. E., Chengalur, J. N., Salpeter, E. E., & Terzian, Y. 1997, *AJ*, 114, 77
- Norman, C., Bowen, D. V., Heckman, T., Blades, C., & Danly, L. 1996, *ApJ*, 472, 73
- O'Donnell, J. E. 1994, *ApJ*, 422, 1580
- Pietz, J., Kerp, J., Kalberla, P.M.W., Burton, W.B., Hartmann, D. & Mebold, U. 1998, *A&A*, 332, 55
- Sakamoto, K., Scoville, N. Z., Yun, M. S., Crosas, M., Genzel, R., Tacconi, L. J. 1999, *ApJ*, 514, 68
- Sanders, D. B., Scoville, N. Z., Sargent, A. I. & Soifer, B. T. 1988, *ApJ*, 324, L55
- Sanders, D. B., Scoville, N. Z., & Soifer, B. T. 1991, *ApJ*, 370, 158
- Schiminovich, D., van Gorkom, J. H., van der Hulst, J. M., & Kasow, S. 1994, *ApJ*, 423, L101
- Schiminovich, D., van Gorkom, J. H., van der Hulst, J. M., & Malin, D. F. 1995, *ApJ*, 444, L77
- Schiminovich, D., van Gorkom, J. H., & van der Hulst, J. M. 1999, *AJ*, submitted
- Schlegel, D. J., Finkbeiner, D. P. & Davis, M. 1998, *ApJ*, 500, 525.
- Schombert, J. M., Wallin, J. F. & Struck-Marcell, C. 1990, *AJ*, 99, 497
- Schweizer, F. 1978, "The Structure and Properties of Nearby Galaxies", IAU Symp. No. 77, edited by E. M. Berkhuysen and R. Wielebinski (Reidel, Dordrecht), p. 279
- Scoville, N. Z., Sargent, A. I., Sanders, D. B., & Soifer, B. T. 1991, *ApJ*, 366, L5
- Scoville, N. Z., Yun, M. S., & Bryant, P. M. 1997, *ApJ*, 484, 702
- Shoppell, P. L., & Bland-Hawthorn, J. 1998, *ApJ*, 493, 129.
- Simkin S. M., van Gorkom, J. H., Hibbard, J. E., Hong-Jun, S. 1987, *Science*, 235, 1367.
- Smith, B. J. 1994, *AJ*, 107, 1695.
- Smith, B. J., Struck, C., & Pogge, R. W. 1997, *ApJ*, 483, 754.
- Sofue, Y. 1994, *ApJ*, 423, 207.
- Sofue, Y., & Wakamatsu, K. 1993, *A&A*, 273, 79.
- Soifer, B. T., Helou, G., Lonsdale, C. J., Neugebauer, G., Hacking, P., Houck, J. R., Low, F. J., Rice, W., & Rowan-Robinson, M. 1984, *ApJ*, 283, L1
- Spitzer, L. 1956, *ApJ*, 124, 20.
- Stanford, S. A., & Balcells, M. 1991, *ApJ*, 370, 118
- Stockton, A. 1974a, *ApJ*, 187, 219
- Stockton, A. 1974b, *ApJ*, 190, L47
- Stockton, A. & Bertola, F. 1980, *ApJ*, 235, 37
- Strickland, D. K., Ponman, T. J., & Stevens, I. R. 1997, *A&A*, 320, 378
- Struck, C. 1997, *ApJ (Supp.)*, 113, 269
- Struck-Marcell, C. 1990, *AJ*, 99, 71
- Suchkov, A. A., Berman, V. G., Heckman, T. M. & Balsara, D. S., 1996, *ApJ*, 463, 528
- Suchkov, A. A., Balsara, D. S., Heckman, T. M., Leitherer, C. 1994, *ApJ*, 430, 511
- Toomre, A., & Toomre, J. 1972, *ApJ*, 178, 623
- van Gorkom, J. H. 1993, in "The Evolution of Galaxies and their Environment", edited by H. A. Thronson and J. M. Shull (Kluwer, Dordrecht), p. 345
- Vogler, A., & Pietsch, W. 1996, *A&A*, 311, 35
- Wallin, J. F. 1990, *AJ*, 100, 1477
- Wang, B. 1995, *ApJ*, 444, 590
- Wang, Q. D., Walterbos, R. A. M., Steakley, M. F., Norman, C. A. & Braun, R. 1995, *ApJ*, 439, 176
- Weil, M. L., & Hernquist, L. 1993, *ApJ*, 405, 142
- Weliachew, L., Sancisi, R., & Guelin, M. 1978, *A&A*, 65, 37
- Wevers, B. H. M. R., Appleton, P. N., Davies, R. D., & Hart, L. 1984, *A&A*, 140, 125
- Yun, M. S. 1992, Ph.D. Thesis, Harvard University
- Yun, M. S. 1997, in "Galaxy Interactions at Low and High Redshift", IAU Symposium No. 186, eds. D. Sanders & J. Barnes, in press
- Yun, M. S., Ho, P. T. P., & Lo, K. Y. 1993, *ApJL*, 411, L17
- Yun, M. S., Ho, P. T. P., & Lo, K. Y. 1994, *Nature*, 372, 530
- Yun, M. S. & Hibbard, J. E. 2000, in preparation
- Yun, M. S. & Hibbard, J. E. 1999, *ApJ*, submitted

TABLE 1
EFFECTS OF RAM PRESSURE AND IONIZATION ON TIDAL MATERIAL

Parameter	Units	NGC 520	Arp 299	Arp 220	notes
V_{hel}	(km s ⁻¹)	2260	3080	5400	
D	(Mpc)	30	48	79	<i>a</i>
L_{IR}	(L _⊙)	7.6×10^{10}	8.1×10^{11}	1.5×10^{12}	<i>b</i>
$N_{HI,max}$	(cm ⁻²)	5×10^{20}	4×10^{20}	4×10^{20}	<i>c</i>
$\sigma_{HI,max}$	(km s ⁻¹)	16	20	40	<i>c</i>
r	(kpc)	25	70	30	<i>d</i>
R_{RRPS}	(kpc)	50	140	95	<i>e</i>
R_{ionize}	(kpc)	25	95	130	<i>f</i>

^aAdopting the distances from Sanders, Scoville & Soifer (1991), which assumes $H_o=75$ km s⁻¹ Mpc⁻¹ and the Virgo-centric flow model of Aaronson *et al.* (1982).

^b8–1000 μ m luminosity, from Sanders, Scoville, & Soifer (1991).

^cMaximum values of gas column density and line-of-sight velocity dispersion observed within the tidal features, taken from HvG96 (NGC 520), HY99 (Arp 299) and Yun & Hibbard 1999a (Arp 220).

^dThe projected radius of “missing” HI.

^eCalculated via eqn. (4), assuming the values given in this table and $dL=10$ kpc.

^fCalculated via eqn. (6), assuming the values given in this table and $f_{esc}(\Omega_{wind})=0.1$ and $dL=10$ kpc.